REPORT DOCUMENTATION PAGE

Form Approved
OMB NO. 0704-0188

1. AGENCY USE ONLY (Leave Blank)	2. REPORT DATE	3. REPORT TYPE AND DATES COVERED
	December 2, 2002	Final, 1/1/1998-4/30/2002

4. TITLE AND SUBTITLE
Experimental Study of the Structure of Shock-Induced Turbulent Separated Flow and Its Role in Flowfield Unsteadiness

5. FUNDING NUMBERS
Grant
DAAG55-98-1-0290

6. AUTHOR(S)
David S. Dolling and Noel T. Clemens

7. PERFORMING ORGANIZATION NAME(S) AND ADDRESS(ES)
The University of Texas at Austin

8. PERFORMING ORGANIZATION REPORT NUMBER

9. SPONSORING / MONITORING AGENCY NAME(S) AND ADDRESS(ES)
U. S. Army Research Office
P.O. Box 12211
Research Triangle Park, NC 27709-2211

10. SPONSORING / MONITORING AGENCY REPORT NUMBER
Proposal #37798-EG

11. SUPPLEMENTARY NOTES
The views, opinions and/or findings contained in this report are those of the author(s) and should not be construed as an official Department of the Army position, policy or decision, unless so designated by other documentation.

12 a. DISTRIBUTION / AVAILABILITY STATEMENT
Approved for public release; distribution unlimited.

12 b. DISTRIBUTION CODE

13. ABSTRACT (Maximum 200 words)

This project was aimed at understanding the fundamental cause of the low frequency unsteadiness present in shock-induced turbulent separated flows. A particular emphasis was placed on investigating the role that the upstream boundary layer plays in driving the motion of the separated flow. Three different interactive flows were studied, which included interactions generated by Mach 2 and 5 unswept compression ramps a Mach 5 blunt fin. This study emphasized the use of imaging techniques -- such as planar laser scattering and particle image velocimetry (PIV) -- to monitor the conditions in the upstream turbulent boundary layer. For the first time in a shock-induced separated flow, a new multi-camera, multi-laser PIV system was used that enabled both wide-field PIV and time-sequenced PIV measurements to be made. Velocity fluctuations in the lower part of the upstream boundary layer were found to be strongly correlated with shock foot motion. This same correlation was demonstrated in both compression ramp and blunt fin interactions. In corroboration of this mechanism, pulsed jet injection was used in the upstream boundary layer to show that the shock can be made to respond to changes in the velocity field induced by the pulsed jets.

14. SUBJECT TERMS	15. NUMBER OF PAGES
Fluid dynamics, turbulence, supersonic flow	22
	16. PRICE CODE

17. SECURITY CLASSIFICATION OR REPORT	18. SECURITY CLASSIFICATION ON THIS PAGE	19. SECURITY CLASSIFICATION OF ABSTRACT	20. LIMITATION OF ABSTRACT
UNCLASSIFIED	**UNCLASSIFIED**	**UNCLASSIFIED**	**UL**

REPORT DOCUMENTATION PAGE

Form Approved OMB No. 0704-0188

1. REPORT DATE (DD-MM-YYYY)	2. REPORT TYPE	3. DATES COVERED (FROM - TO)
02-12-2002		01-01-1998 to 30-04-2002

4. TITLE AND SUBTITLE
Experimental Study of the Structure of Shock-Induced Turbulent Separated Flow and Its Role in Flowfield Unsteadiness
Unclassified

5a. CONTRACT NUMBER
5b. GRANT NUMBER
5c. PROGRAM ELEMENT NUMBER

6. AUTHOR(S)

5d. PROJECT NUMBER
5e. TASK NUMBER
5f. WORK UNIT NUMBER

7. PERFORMING ORGANIZATION NAME AND ADDRESS
University of Texas
Austin
Austin, TX78701

8. PERFORMING ORGANIZATION REPORT NUMBER

9. SPONSORING/MONITORING AGENCY NAME AND ADDRESS
,

10. SPONSOR/MONITOR'S ACRONYM(S)
11. SPONSOR/MONITOR'S REPORT NUMBER(S)

12. DISTRIBUTION/AVAILABILITY STATEMENT
APUBLIC RELEASE
,

13. SUPPLEMENTARY NOTES

14. ABSTRACT

This project was aimed at understanding the fundamental cause of the low frequency unsteadiness present in shock-induced turbulent separated flows. A particular emphasis was placed on investigating the role that the upstream boundary layer plays in driving the motion of the separated flow. Three different interactive flows were studied, which included interactions generated by Mach 2 and 5 unswept compression ramps a Mach 5 blunt fin. This study emphasized the use of imaging techniques -- such as planar laser scattering and particle image velocimetry (PIV) -- to monitor the conditions in the upstream turbulent boundary layer. For the first time in a shock-induced separated flow, a new multi-camera, multi-laser PIV system was used that enabled both wide-field PIV and timesequenced PIV measurements to be made. Velocity fluctuations in the lower part of the upstream boundary layer were found to be strongly correlated with shock foot motion. This same correlation was demonstrated in both compression ramp and blunt fin interactions. In corroboration of this mechanism, pulsed jet injection was used in the upstream boundary layer to show that the shock can be made to respond to changes in the velocity field induced by the pulsed jets.

15. SUBJECT TERMS

16. SECURITY CLASSIFICATION OF:			17. LIMITATION OF ABSTRACT	18. NUMBER OF PAGES	19. NAME OF RESPONSIBLE PERSON
a. REPORT	b. ABSTRACT	c. THIS PAGE	Public Release	23	Rike, Jack jrike@dtic.mil
Unclassified	Unclassified	Unclassified			19b. TELEPHONE NUMBER International Area Code Area Code Telephone Number DSN

Standard Form 298 (Rev. 8-98)
Prescribed by ANSI Std Z39.18

REPORT DOCUMENTATION PAGE (SF298)
(Continuation Sheet)

Table of Contents

Problem Statement

A flow of particular interest to the U.S. Army is shock-wave induced turbulent boundary layer separation which occurs around missile fins, base flows and rotor blades. A common feature of these flows is that they are highly unsteady and are characterized by large-scale pulsation at frequencies that are an order of magnitude, or more, below the characteristic frequency of the turbulence. Due to the complex nature of these flows and the high Reynolds numbers at which they exist, they remain largely beyond the capabilities of current theoretical and computational techniques. Therefore, at this stage, it is unlikely that they key phenomena and mechanisms responsible for the flowfield unsteadiness will emerge solely from computation. This highlights the crucial role that advanced measurements must play if a fundamental understanding of the physics of such complex flowfields is to be attained.

This project was aimed at understanding the fundamental cause of the low frequency unsteadiness present in shock-induced turbulent separated flows. A particular emphasis was placed on investigating the role that the upstream boundary layer plays in driving the motion of the separated flow. In order to determine the universality of any effects observed, three different interactive flows were studied, which included interactions generated by: 1) unswept compression ramps in Mach 2 and Mach 5 flows, and 2) a blunt fin in a Mach 5 flow. This study emphasized the use of imaging techniques -- such as planar laser scattering and particle image velocimetry (PIV) -- to monitor the conditions in the upstream turbulent boundary layer. The unsteadiness of the separated flow was simultaneously characterized by using wall-mounted fast response pressure transducers. For the first time in a shock-induced separated flow, a new multi-camera, multi-laser PIV system developed at UT-Austin was used. This system enabled both wide-field PIV and time-sequenced PIV measurements to be made, which represents a significant advance over measurements that have been made to date. Wide-field PIV enabled imaging of the velocity field spanning the upstream turbulent boundary layer, intermittent region, separated flow, and the region of reattachment on the ramp face.

In this study it was found that velocity fluctuations in the upstream boundary layer were strongly correlated with shock foot motion. This correlation was strongest for fluctuations in the lower third of the boundary layer. This same correlation was demonstrated in both compression ramp and blunt fin interactions, which indicates it may be a universal mechanism and not just restricted to a certain type of flow geometry. As a further test of this mechanism, pulsed jet injection was used in the upstream boundary layer to determine if the shock would respond to changes in the velocity field induced by the pulsed jets. In agreement with the previous results, the shock foot was found to move downstream when the state of the jets went from on to off, whereas it moved upstream when the jets went from off to on. These results offer strong corroborating evidence that upstream velocity fluctuations influence the shock motion and that it may be possible to control the unsteadiness to mitigate many of the problems associated with shock-induced separation.

Participating Personnel

David S. Dolling - Professor

Noel T. Clemens - Associate Professor

Ö. Haldun Ünalmis – Research Associate

Steven Beresh - Graduate Research Assistant, Ph.D. 1999

Roderick Austin – Graduate Research Assistant, M.S. 2001

Yongxi Hou – Graduate Research Assistant, Ph.D expected 2003

Publications and Technical Reports

1. Beresh, S.J., "The Effect of the Incoming Turbulent Boundary Layer on a Shock-Induced Separated Flow Using Particle Image Velocimetry" Ph.D. Dissertation, The University of Texas at Austin, 1999.

2. Comninos, M., "Investigations into the Causes of Shock Wave / Turbulent Boundary Layer Interactions using Planar Laser Scattering" M.S. Thesis, The University of Texas at Austin, 1997.

3. Austin, R., "Effect of Upstream Pulsed Mass Injection on a Mach 2 Shock-Wave / Turbulent Boundary Layer Interaction" M.S. Thesis, The University of Texas at Austin, 2001

4. Beresh, S.J., M. Comninos, N. T. Clemens and D.S. Dolling, "The Effects of the Incoming Turbulent Boundary Layer Structure on a Shock-Induced Separated Flow," AIAA 98-0620, 36th Aerospace Sciences Meeting, Reno, NV, 1998.

5. Beresh, S.J., Clemens, N.T. and Dolling, D.S., "The relationship between upstream turbulent boundary layer velocity fluctuations and separation shock unsteadiness," AIAA 99-0295, 37th Aerospace Sciences Meeting, 1999.

6. D.S. Dolling, "*50 Years of Shock Wave/Boundary Layer Interaction – What Next?,*" AIAA Journal, Vol. 39, No. 8, pp. 1517-1531 (2001).

7. Beresh, S. J., N. T. Clemens and D.S. Dolling, "The Relationship Between Upstream Turbulent Boundary Layer Velocity Fluctuations and Separation Shock Unsteadiness" AIAA Journal (to be published, December 2002).

8. Ünalmis, Ö. H., Hou, Y. X., Clemens, N. T., Dolling, D. S. and Bueno, P. C., "PIV Investigation of Role of Boundary Layer Velocity Fluctuations in Unsteady Shock-Induced Separation," AIAA paper 2450, 21st Advanced Technology and Ground Testing Conference, June 2000 (invited).

9. Hou, Y.X., Clemens, N.T. & Dolling, D.S., "Time-Sequenced PIV Imaging of a Shock/Boundary Layer Interaction," AIAA paper 2002-3232, June 2002.

Summary of Results

Background

Work in a broad range of supersonic separated turbulent flows has suggested that the separation shock foot motion and the expansion/contraction (or pulsation) of the separated flow can be described as a low frequency, large-scale motion superimposed on which is a high frequency, small-scale motion.[1-11] Figure 1a shows an example of the separation shock foot position history deduced from wall pressure signals in an unsteady, separated, unswept compression ramp flow at Mach 5 (shown in Fig. 1b), clearly exhibiting the broad range of motions and frequencies present in the shock foot behavior.

Erengil and Dolling's[9] studies of separation shock foot unsteadiness showed a correlation between the wall pressure fluctuations beneath the incoming boundary layer and the shock foot velocity, from which it was inferred that the small-scale motion of the shock is caused by its response to the convection of turbulent fluctuations through the interaction. Their work also demonstrated that the large-scale motion is a result of the shock's displacement due to the expansion and contraction of the separation bubble. A physical model of the shock unsteadiness can be produced from these observations, where the expansion and contraction of the separation bubble displaces the shock upstream or downstream, while the passage of turbulent fluctuations alters the shock velocity, which integrates to changes in the shock position and accounts for the small-scale high-frequency unsteadiness. While this model offers an explanation for the small-scale motion and a limited explanation for the large-scale motion, it does not address what causes the separation bubble to undergo its low-frequency, large-scale pulsation.

To address this question, McClure[5] and Ünalmis and Dolling[12] made conditional Pitot pressure measurements in the upstream boundary layer and determined that the mean Pitot pressure at a fixed vertical position was lower for upstream shock locations than for downstream shock locations. This observation led to a simple model in which low-frequency variations in the incoming boundary layer *thickness* induce the large-scale shock motion. Chan[13] and Beresh et al.[14] further examined this thickening/thinning mechanism using planar laser imaging techniques. Instantaneous planar laser scattering (PLS) from a condensed alcohol fog was used to obtain images upstream of the interaction in the incoming undisturbed boundary layer simultaneous with pressure signals from transducers used to track the shock foot motion. When analyzed to determine the local mean boundary layer thickness just upstream of the interaction region, the PLS images exhibited no significant correlation between this parameter and the shock location.

Beresh et al.[14] additionally acquired particle image velocimetry (PIV) images simultaneous with pressure data, similar to the PLS experiment. The resulting vector fields were ensemble averaged based upon the shock foot location as determined from the pressure data, producing conditional mean velocity profiles through the boundary layer. No measurable difference in the boundary layer thickness was found corresponding to different shock foot positions, but the profiles suggested a small difference in the profile shape that may correlate with the shock foot location. When the PLS and PIV data are considered as a whole, they provide little support for the "thickening/thinning" boundary layer concept as a means of explaining the low-frequency motion of the separation shock. Thus the systematic variations in the boundary layer Pitot pressure, which correlate with the separated flow scale, were apparently not due to low-frequency variations in the upstream boundary layer thickness.

Study Objectives

The discussion above indicates that although a great deal of work has been directed at this issue, the fundamental cause of the low frequency unsteadiness of shock-induced turbulent separation was not known at the time that this research program was initiated. Our work that was supported by a previous ARO grant indicated that the low frequency unsteadiness was not caused by a thickening/thinning of the upstream boundary layer, and preliminary results showed that turbulent fluctuations in the upstream boundary layer may be correlated with the motion of the shock foot. The primary objective of this work was to investigate these findings in more detail and to make a definitive study on the role of the upstream turbulent boundary layer velocity fluctuations on the separation shock foot motion.

One of the major results of this study was that we identified a clear correlation between velocity fluctuations in the near-wall region of the upstream boundary layer and shock foot motion. A second objective was to show that this correlation may be universal, to the extent that it exists in different flow geometries. To accomplish the latter, experiments were conducted in both compression ramp and blunt fin interactions. As an independent means of showing the role of upstream velocity fluctuations on the shock motion, velocity perturbations were purposefully introduced into the flow by using pulsed air jet injection upstream of the interaction. The objective of these experiments was to determine if transitions in the state of jet injection (e.g. transitions from on to off) would lead to shock motion in accord with what could be inferred from the previous measurements. Another objective of this work was to investigate possible driving mechanisms of flow unsteadiness that may originate in the separated flow region downstream of the separation shock. Toward this end, a major effort was directed at developing a new multi-camera, multi-laser PIV system that enables us to acquire either wide field of view PIV or time-sequenced velocity data. The wide field of view imaging enables the simultaneous imaging of the entire interaction – i.e. the upstream turbulent boundary layer, the intermittent region, the separated flow and the reattachment region on the ramp face – which has proven extremely useful for understanding the instantaneous flow structure.

EXPERIMENTAL APPARATUS AND PROCEDURE

Experimental Facility

All experiments were performed in the Mach 2 and 5 blowdown wind tunnel at the University of Texas at Austin. The test section has a constant cross-sectional area of 7×6 in^2 and is equipped with two nozzle blocks to enable test section Mach numbers of 2 and 5. The freestream unit Reynolds numbers were 15.1×10^6 ft^{-1} and 10×10^6 ft-1 at Mach 5 and 2, respectively. After transitioning naturally, the incoming boundary layer in the test section was fully turbulent and developed under nearly adiabatic wall temperature flow conditions. The interactions that were studied were generated by: 1) an unswept full-span 28-degree compression ramp at Mach 5, 2) a blunted fin with a 0.75 *in* leading edge diameter at Mach 5, and 3) a non-full-span 20-degree compression ramp at Mach 2. Schematic diagrams of the 28 degree compression ramp and blunt fin installed on the floor of the test section are shown in Fig. 1b and 2, respectively.

Fluctuating Pressure Measurements

The pressure measurements were made using fast response transducers (Kulite model XCQ-062-50A) flush-mounted into a plug that was inserted into the floor of the test section. The transducers had a frequency response of about 50 kHz. The output from each transducer was low-pass filtered at 50 kHz and digitized to 12 bits at 100 kHz by an analog-to-digital converter (LeCroy 6810). Two different transducer arrangements were used, both incorporating five transducers. The first configuration aligned all five transducers in the streamwise direction with a center-to-center spacing of 0.115" (2.92 mm) while the second configuration used a staggered arrangement consisting of one row of two transducers adjacent to a row of three transducers. In the latter case, the row of two transducers is offset in the streamwise direction from the row of three transducers by one-half of a transducer spacing, providing an effective streamwise transducer spacing of 0.058" (1.46 mm). Neither arrangement is sufficient to fully span the length of the intermittent region (the range within which the shock foot moves), so the compression ramp can be moved with respect to the pressure transducers to allow pressure measurements at different locations within the intermittent region for different experimental runs. The fluctuating pressure signals were reduced to measurements of the shock foot location using the algorithms detailed by Dolling and Brusniak[3] and Gramann and Dolling.[5]

Pulsed Jet Injection Setup

The pulsed jets were produced by using six fast-acting solenoid valves (General Valve, Iota One), flush mounted on the tunnel floor just upstream of the interaction as shown in Fig. 3. The response time of the valves is about 1 ms. The valves have a 2 mm orifice and can deliver approximately 20 standard liters per minute of air per valve when pressurized to 12 atm. The six injectors were operated at 100 Hz. The shock motion was monitored by using flush mounted pressure transducers underneath the intermittent region as described above.

Conventional Particle Image Velocimetry

The conventional PIV image acquisition system that was used for most of the work in this project is shown in Figure 4. The light source was a dual-cavity Nd:YAG laser (Spectra Physics Quanta-Ray PIV-400) operated at 10 Hz and 50 mJ per pulse. The scattered laser light was collected with a "frame-straddling" 1000 × 1000 pixel CCD camera (Kodak MegaPlus ES 1.0), which enabled the acquisition of each laser pulse in a separate frame. Analysis of the image data was performed by using PIV software developed in-house. This proprietary software provided several advantages over commercially available software including optimization of offsets between exposures for cross-correlations and optional particle tracking to improve spatial resolution.

The seed particles used were made of aluminum oxide and had a mean particle size of about 1.0 μm. The particles were delivered using a two stage seeder; the first stage was a dual fluidized bed, where two cylinders operated in parallel to entrain the particles in an air flow by driving the flow through a bed of particles. Both fluidized beds tangentially fed into a cyclone separator that formed the second stage, which was designed to separate and dispose of the heavier particles due to the larger centrifugal force applied to them. For the Mach 5 studies, a streamlined local injector delivered the particles into the flow at the exit plane of the nozzle. The injector was 0.6" in height, 0.55" wide, and 4.3" long in the streamwise direction; the leading and trailing edge surfaces were swept towards the center of the injector, yielding an appearance akin

to a tapered diamond shape. It was located 31" upstream of the compression ramp corner, just upstream of the exit plane of the nozzle. For the Mach 2 studies, the particles were seeded into the plenum, not into the test section.

Multi-Camera, Multi-Laser PIV System

The multi-camera, multi-laser PIV system is shown schematically in Fig. 5. The light source for the system is a pair of dual-cavity, Nd:YAG lasers (Spectra-Physics PIV-400), where each of the cavities (4 in total) can be double-pulsed. Between the two lasers, a pulse train of eight laser pulses can be generated, where the pulse train is repeated at a rate of 10 Hz. The maximum energy per pulse is about 40 mJ for each of the eight pulses. The output beam from the two separate lasers is combined into a single co-linear beam that is then directed to the test section. The pulse train produced by the lasers depends on whether the system is used for wide-field imaging or time-sequenced imaging. For wide-field imaging, four cameras (Kodak ES1.0), of resolution 1k×1k pixels, are positioned to image a region of area 21.6×21.6 mm^2, to give a total field of view that was 86 *mm* long by 21.6 *mm* high. To enable the cameras to image overlapping fields-of-view without tilting them, two pairs of cameras were located on opposite sides of the test section, and each pair imaged the flow through a cubic beam splitter. In this case, all cameras imaged the same laser sheet, which was double-pulsed with a time between pulses of 1 μs. For time-sequence imaging, the two cameras were placed on the same side of the test section and imaged the same field-of-view through a cubic beam splitter. Each camera was mounted on an x-y translation stage and a micrometer positioned "tilt" stage that enabled the fields of view to be matched to an accuracy of about a pixel. This level of accuracy was sufficient for the purposes of this study. The two cameras detected particle image pairs separated in time by 40 μs, as compared to the time-between-pulses for each PIV image pair, which was 1 μs.

The scattering for each camera was differentiated by using a ferroelectric liquid crystal (FLC) shutter (DisplayTech FLC Light Valve) in front of each camera. The FLC shutters were 1" diameter and were custom mounted into C-mount to Nikon lens adapters. The open/close time of the shutters is about 20 ~ 30 μs. Several pulse-delay generators (Stanford Research Systems DG535) were used to synchronize the system and to trigger the different components. For the time-sequence imaging, the laser produced 4 laser pulses per cycle of the laser. The pulses were monitored using a fast photodiode connected to a digital oscilloscope (Tektronix TDS 520C).

TECHNICAL ACCOMPLISHMENTS

Correlation of Velocity Fluctuations with Shock Motion -- Compression Ramp Interactions

Large ensembles of high quality PIV measurements were acquired in the upstream boundary layer, simultaneous with separation shock foot location information as inferred from wall mounted pressure transducers. The velocity vector fields were sorted into several conditional groups based upon the motion of the shock foot at the time the imaged region of the flow convected through the intermittent region. Specifically, conditional profiles were obtained based on the distance the separation shock traveled during a specified time window. Example profiles are shown in Fig. 6 for the case where the shock moves 1, 2, or 3 transducers within a time-window of 250 μs (corresponding to a frequency range of 4 kHz and above). From Fig. 6 it is seen that there is little difference in the profiles in the outer region of the boundary layer. Near the wall, however, there is a clear systematic variation of the profiles for the different types of

shock motion. Shocks that exhibit no motion within this time period, on average, are associated with a velocity fluctuation of zero. In contrast, shocks that move upstream are associated with negative velocity fluctuations and the magnitude of the fluctuations increases with larger distances traveled by the shock. Similarly, shocks that move downstream correlate with positive velocity fluctuations. This correlation of negative velocity fluctuations with upstream shock motions and positive velocity fluctuations with downstream shock motions is precisely that shown by the simulations of Hunt and Nixon,[17] although the magnitude of the fluctuations found here is significantly lower.

The magnitude of the velocity fluctuations which exhibit a correlation to the shock motion is on the order of 10 m/s, which initially would appear to surprisingly small since $\sqrt{\overline{u'^2}}$ is about 50 - 80 m/s near the wall. This value might be low due to noise in the correlation, but it does make some physical sense. A shock motion of two transducer spacings is 5.8 mm, and in the 250 Fs time period corresponding to 4 kHz shock motions, the resulting shock velocity is 23 m/s. Thus a fluctuation in the range of 50 - 80 m/s is not necessary to produce this shock motion and while the 10 m/s fluctuations found by the ensemble averages are somewhat low, it is not egregiously implausible. The effects of noise upon the correlation can reasonably account for the reduced velocity.

Correlation of Velocity Fluctuations with Shock Motion – Blunt Fin Interactions

These are very intriguing results as they are the first to offer direct experimental evidence of a relationship between the velocity fluctuations in the upstream boundary layer and the motion of the separation shock foot. However, it is not clear if the observed correlation is a universal mechanism that is present in all shock-induced separated flows, or perhaps is only present in the compression ramp interaction. To address this issue, measurements similar measurements to those described above were made in a blunt-fin interaction. The blunt-fin interaction was chosen because its mean flowfield scales on different parameters than the compression ramp interaction does. For example, the size of the intermittent region (i.e., the region where the separation shock foot unsteadiness occurs) scales on the fin diameter in the blunt-fin interaction, whereas it scales on the boundary layer thickness for the compression ramp interaction. The fact that the mean flowfield of the blunt-fin interaction is largely independent of the scale of the upstream boundary layer, may indicate that the interaction is less sensitive to changes in the upstream boundary layer. Therefore, it might be expected that the correlation seen in the compression ramp interaction between upstream velocity fluctuations and shock motion would be weaker in the blunt-fin interaction.

A schematic diagram of the blunt-fin model mounted in the test section is shown in Fig. 2. The model was a hemicylindrically blunted fin that had a 0.75 in. leading edge diameter and was 4 in. high. As with the compression ramp interaction, the separation shock motion was monitored by several flush mounted fast-response pressure transducers located within the intermittent region. The blunt-fin experiments were conducted in a similar manner to the compression-ramp experiments, where the upstream velocity fluctuations were ensemble averaged for particular types of shock motions. Approximately 5000 PIV images were acquired for these experiments. Example results are shown in Fig. 7 for a 100 μs time window where profiles are shown for the following shock motions: no motion, upstream 1 and 2 transducers, downstream 1 and 2 transducers. The profiles show good agreement with those obtained for the compression ramp interaction, as a correlation is observed between the upstream velocity

fluctuations in the lower part of the boundary layer and shock-foot motion.

These results show that the mechanism of upstream velocity fluctuations inducing shock-foot motion may be a universal aspect of shock-induced separated flows. However, it is not known if this is the only (or even the primary) mechanism at work in such flows. In future work we plan to explore these effects further, in both compression-ramp and blunt-fin interactions, with more sophisticated measurement strategies. For example, it is possible that the separation shock responds not to velocity fluctuations but to flow acceleration in the upstream boundary layer.

Pulsed Jet Injection

Since one of the previous major findings of this research is that the shock motion is correlated with upstream velocity fluctuations, an important question that needs to be addressed is: how sensitive are the shock dynamics to upstream perturbations, and is it possible to control the shock motion by purposefully creating upstream perturbations? To address this question, we conducted a series of experiments that were aimed at investigating the effect of pulsed jet injection into the upstream boundary layer on the separation shock motion.

The experiments and analysis were aimed at understanding what happens to the shock foot when upstream injection is turned on or off. For example, every time injection started, the resulting shock motion was determined, and the movement was categorized as a movement of 0, +/- 1 bin, +/- 2 bins, or +/- 3 bins, where a bin is the distance between the transducers. Figure 8a shows a histogram of shock motions when the injectors transition from off to on. The histogram shows that when injection is started, the shock either remains in the same location, or moves upstream only one bin position. On the other hand, Fig. 8b shows the case where the injection transitions from on to off. In this case, the shock either stays stationary, or moves downstream one bin position. The significance of these results is shown in Fig. 8c, which shows the shock motion for the same injector triggering signal, but where there is no gas injection. In contrast with the cases with injection, shock motions of 0 and +/- 1 bin, are approximately equally probable. These are exciting results because they show that upstream jet injection is having a substantial effect on the resulting shock motion. These results reinforce our previous results that showed that the shock foot responds to velocity fluctuations in the upstream boundary layer. The jet injection introduces a disturbance, and the shock foot responds just as would be inferred from the PIV results discussed above. For example, when the jets are turned on, they inject low (streamwise) momentum fluid into the boundary layer, which in effect, causes a negative velocity fluctuation. From Fig. 6, we would expect this would result in the separation shock moving upstream. This is exactly what we see in Fig. 8a. Similarly, when the jets transition from on to off, this would result in a positive velocity fluctuation, and the shock should move downstream. Again, this is what was shown in Fig. 8b. These results are significant because they suggest that it may be possible to control the interaction dynamics, which could be very useful in the design of high-speed projectiles and aircraft.

Multi-Camera, Multi-Laser PIV Imaging

A new multi-frame PIV imaging system has been developed and applied in a Mach 2 compression ramp interaction. This system enables both “wide-field” and time-sequenced PIV imaging, and represents a major advance in our ability to study these complex flows. Figure 9 shows a composite of four single-pulse particle scattering images for the wide-field PIV taken with a 20 degree ramp. The upstream boundary layer, whose thickness is shown on the image, is

seen in the left half of the composite as a region of less uniform particle density. Furthermore, the separation shock can be seen as a diagonal “blurry” region (as in Fig. 9) near the center of the figure. The particle density is excellent for PIV, even in what is expected to be the region of separated flow, which in the mean should extend from just downstream of the shock until about half a boundary layer thickness up the ramp face. The individual images that compose a composite image are taken at the same time.

Figure 10 shows the instantaneous velocity vector field that was derived from the particle field of Fig. 9. A careful viewing of Fig. 10 shows that these large field-of-view images provide an astounding amount of information about the global structure of the interaction. In the instantaneous images a relatively abrupt flow deflection, presumably across the separation shock, can be seen in the image. To help the reader identify the shock, the locus of points where the vectors first begin to deflect upwards was identified “by eye” and is shown as the solid line in each image. From Fig. 10 it is seen that upstream of the shock, the vectors exhibit very little variation in angle or magnitude and indicate the velocity fluctuations are only a few percent of the free stream velocity. Downstream of the shock, the vectors exhibit substantially more variation. What is presumably the separated flow region can also be seen as a region of low velocity. In the case of Fig. 10, the separated flow seems to originate just downstream of the separation shock foot, whereas in other cases it can originate substantially downstream of the shock foot. We also observe that in the separated flow region, the reverse velocities tend to be relatively small, although in some cases reverse velocities as high as 100-200 m/s are observed. We do not know, however, if the lack of reversed flow is related to the fact that our compression ramp is not full span, and therefore the 3-D relieving effect may weaken the interaction and hence the strength of recirculation. We also observe that the region of “reattachment” exhibits wide variation in its structure. In the majority of images no point of reattachment can be identified at which the flow diverges on each side of it.

The velocity fluctuation fields, computed by subtracting the instantaneous images of Fig. 10 from the mean vector field, are shown in Fig. 11. In the fluctuation fields, the separation shock can often be identified easier than with the instantaneous images, because it often appears as a line to which the velocity vectors exhibit a perpendicular orientation. This characteristic of the fluctuation fields is primarily due to the fact that the shock is highly unsteady. The fluctuations are seen to be relatively small upstream of the shock, but significantly larger downstream of it. It appears that the maximum fluctuations occur in the shear layer that bounds the separated flow, and in the reattaching boundary layer that is forming on the ramp face. This amplification of fluctuations owing to the compression process has been established in earlier studies that have used conventional diagnostics. In Fig. 11, all of the fluctuation vectors downstream of the shock point in the upstream direction. As seen in Fig. 11, this is because the separated flow appears to be very large, which leads to a large region of stagnant fluid downstream of the shock. The fluctuations seem to even penetrate upstream to the location of the shock foot. This type of image brings up the obvious question of "do the downstream fluctuations influence the shock foot or *vice-versa*?" Previous work has suggested that velocity fluctuations in the upstream boundary layer are indeed correlated with the shock foot motion, but it is not known if other, perhaps more dominant, mechanisms may also be present.

Sample time-sequence velocity vector fields obtained with a time delay of 40 μs are shown in Fig. 12. The field of view captures part of the separation shock and region of separated flow, but typically not the separation shock foot. In 40 μs, fluid traveling at the freestream velocity of 500 m/s will travel a distance of 20 mm, i.e. nearly across the entire image, which is 21.6 mm wide. Fluid that is traveling slower than this, such as that in the boundary layer or separated flow, should not convect as far. From the sample images of Fig. 12 we can make some

interesting, if not completely understood, observations about the characteristics of the flow. For example, near the vertical middle of the image it is seen that the velocity vector angle after the shock in Fig. 12 is substantially different in each image. Furthermore, although the shock foot cannot be seen in these images, the separation shock does seem to undergo a great deal of distortion in 40 μs. In fact, the large amount of shock distortion can be seen in all three of the image pairs. The large amount of separation shock distortion by turbulent structures is qualitatively consistent with what have been observed by using PLS imaging. However, in Ref. 15, the PLS visualizations in Mach 5 compression ramp interactions showed that although the outer part of the shock would be greatly distorted by upstream turbulent structures, the shock foot did not move appreciably in 15-30 μs. At this time, it is not clear if our current observations are inconsistent with these previous results. It is possible that the lines drawn on Fig. 12, which indicate the location where the vectors first begin to deflect, may not accurately indicate the location of the shock, particularly in regions of high turbulence. In future experiments, fast-response wall pressure measurements underneath the shock foot will be made simultaneously with the PIV time sequences in order to investigate this issue.

CONCLUSIONS

During the course of this project we have made significant progress toward achieving the goals of the original proposal. The major contribution of this study has been that we have identified, for the first time, a strong correlation between velocity fluctuations in the upstream boundary layer and separation shock foot motion. This correlation indicates that upstream perturbations represent a major source of the separation shock foot unsteadiness. This effect was demonstrated in both compression ramp and blunt fin interactions, and indicates that the observed mechanism may be a universal one. Another significant finding was that pulsed mass injection upstream of the interaction can have a strong effect on shock foot motion. These results represent further confirmation that the shock foot responds to velocity fluctuations in the upstream boundary layer. Furthermore, the pulsed injection results are significant because they suggest that it may be possible to control the interaction dynamics, which could be very useful in the design of high-speed projectiles and aircraft. Finally, we have developed a new multi-frame PIV imaging system that represents a significant advance in our ability to study high-speed turbulent flows.

Bibliography

1 Gramann, R.A. and Dolling, D.S., "Dynamics of Separation and Reattachment in a Mach 5 Unswept Compression Ramp Flow," AIAA Paper 90-0380, January, 1990.

2 Andreopoulos, J. and Muck, K.C., "Some New Aspects of the Shock-Wave/Boundary-Layer Interaction in Compression Ramp Flows," Journal of Fluid Mechanics, Vol. 180, 1987, pp. 405-428.

3 Dolling, D.S. and Brusniak, L., "Separation Shock Motion in Fin, Cylinder, and Compression Ramp Induced Turbulent Interactions," AIAA Journal, Vol. 27, No. 6, 1989, pp. 734-742.

4 Marshall, T.A., and Dolling, D.S., "Computation of Turbulent, Separated, Unswept Compression Ramp Interactions," AIAA Journal, Vol. 30, No. 8, 1992, pp.2056-2065.

5 Gramann, R.A., and Dolling, D.S., "Detection of Turbulent Boundary-Layer Separation Using Fluctuating Wall Pressure Signals," AIAA Journal, Vol. 28, No. 6, 1990, pp. 1052-1056.

6 Erengil, M.E. and Dolling, D.S., "Correlation of Separation Shock Motion with Pressure Fluctuations in the Incoming Boundary Layer," AIAA Journal, Vol. 29, No. 11, 1991, pp. 1868-1877.

7 Erengil, M.E. and Dolling, D.S., "Unsteady Wave Structure near Separation in a Mach 5 Compression Ramp Interaction," AIAA Journal, Vol. 29, No. 5, 1991, pp. 728-735.

8 McClure, W.B., "An Experimental Study of the Driving Mechanism and Control of the Unsteady Shock Induced Turbulent Separation in a Mach 5 compression Corner Flow," Ph.D. Dissertation, Dept. of Aerospace Engineering and Engineering Mechanics, The University of Texas at Austin, August 1992.

9 Erengil, M.E. and Dolling, D.S., "Physical Causes of Separation Shock Unsteadiness in Shock Wave/Turbulent Boundary Layer Interactions," AIAA Paper 93-3134, July, 1993.

10 Brusniak, L., and Dolling, D.S., "Physics of Unsteady Blunt-Fin-Induced Shock Wave / Turbulent Boundary Layer Interactions," Journal of Fluid Mechanics, Vol. 273, 1994, pp. 375-409.

11 Dolling, D.S., "Fluctuating Loads in Shock Wave/Turbulent Boundary Layer: Tutorial and Update," AIAA Paper 93-0284, January 1993.

12 Ünalmis, O.H. and Dolling, D.S., "Decay of Wall Pressure Field and Structure of a Mach 5 Adiabatic Turbulent Boundary Layer," AIAA Paper 94-2363, June, 1994.

13 Chan, S.C., "Planar Laser Scattering Imaging of Shock Wave Turbulent Boundary Layer Interactions," M.S. Thesis, Dept. of Aerospace Engineering and Engineering Mechanics, The University of Texas at Austin, November 1996.

14 Beresh, S.J., Clemens, N.T., Dolling, D.S., and Comninos, M., "Investigation of the Causes of Large-Scale Unsteadiness of Shock-Induced Separated Flow Using Planar Laser Imaging," AIAA Paper 97-0064, January, 1997.

15 Beresh, S.J., Comninos, M., Clemens, N.T., and Dolling, D.S., "The Effects of the Incoming Turbulent Boundary Layer Structure on a Shock-Induced Separated Flow," AIAA Paper 98-0629, January, 1998.

16 Beresh, S.J., Clemens, N.T. and Dolling, D.S., "The relationship between upstream turbulent boundary layer velocity fluctuations and separation shock unsteadiness," AIAA 99-0295, 37th Aerospace Sciences Meeting, 1999

17 Hunt, D., and Nixon, D., "A Very Large-Eddy Simulation of an Unsteady Shock Wave / Turbulent Boundary Layer Interaction," AIAA Paper 95-2212, 1995.

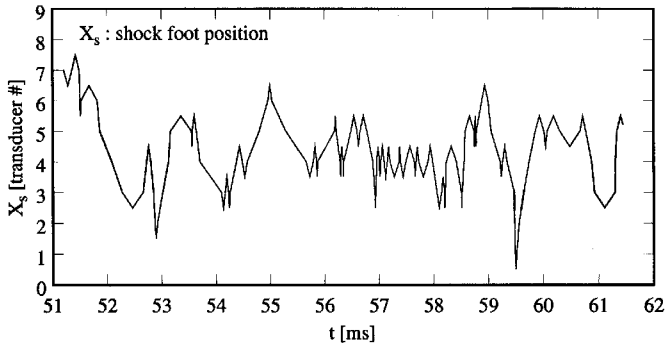

(a)

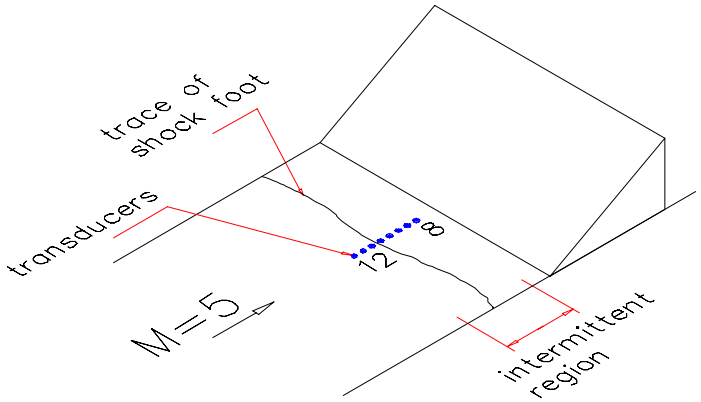

(b)

Figure 1. Sample shock foot position history obtained in a Mach 5 compression ramp interaction shown in (a). The compression ramp and transducers located under the intermittent region are shown in (b).

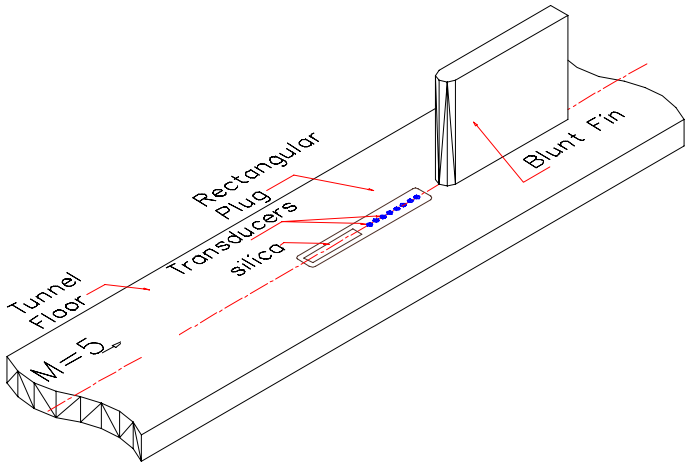

Figure 2. Schematic diagram of the blunt fin model installed in the Mach 5 wind tunnel.

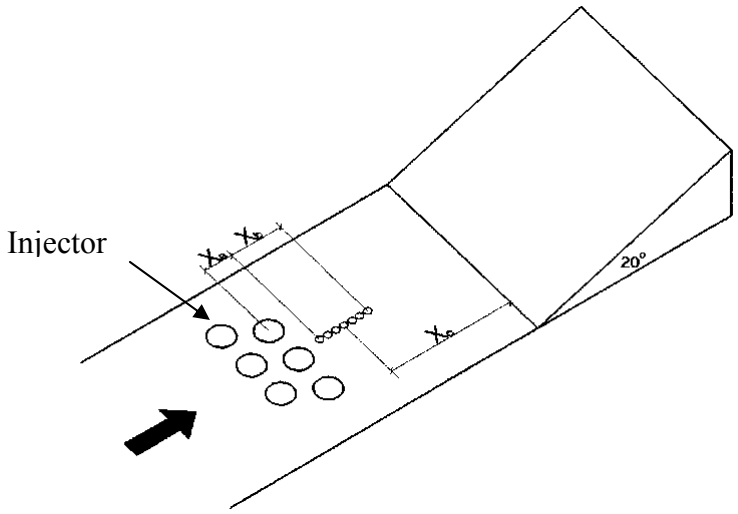

Figure 3. Schematic of the Mach 2 compression ramp and the pulsed jet injectors that are mounted in the floor of the wind tunnel. The six injectors have a 2 mm orifice diameter and can be actuated independently or in concert.

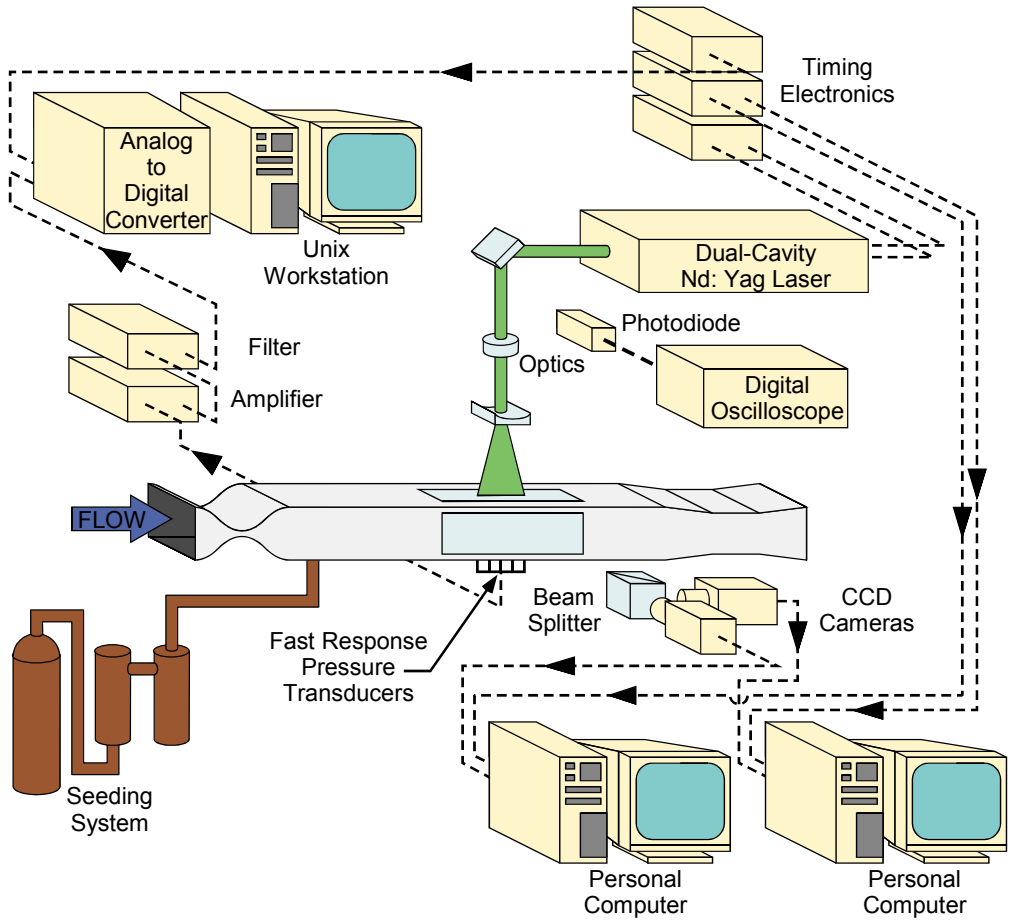

Figure 4. Schematic conventional PIV setup for studies of compression ramp and blunt fin interactions.

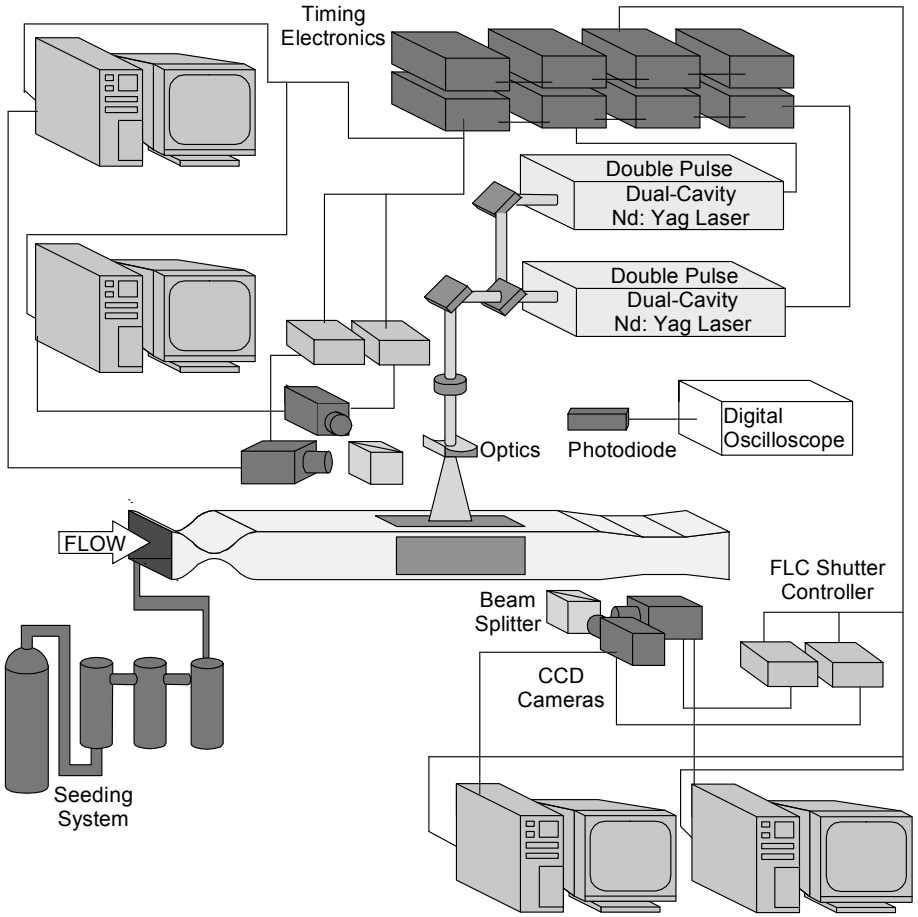

Figure 5. Schematic of the multi-camera, multi-laser PIV system setup.

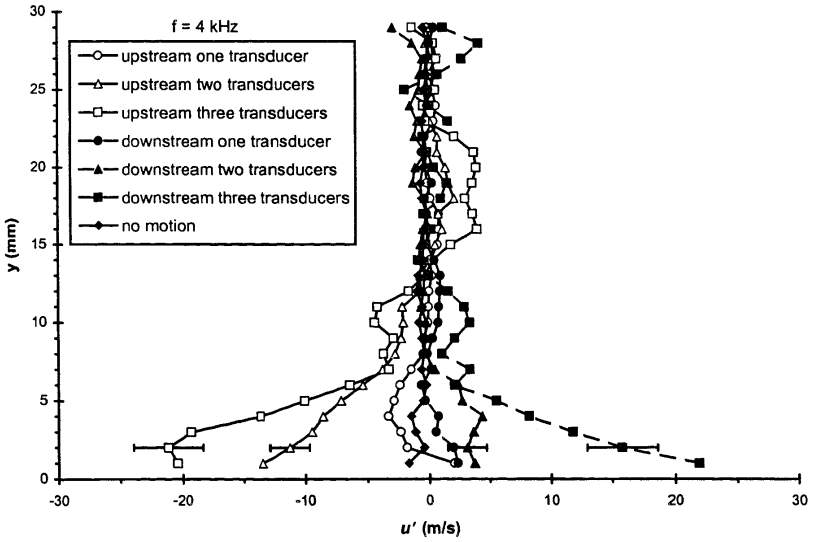

Figure 6. Conditional ensemble average profiles of the streamwise velocity fluctuations in the incoming boundary layer conditioned upon the separation shock foot motion within a time period corresponding to 10 kHz:

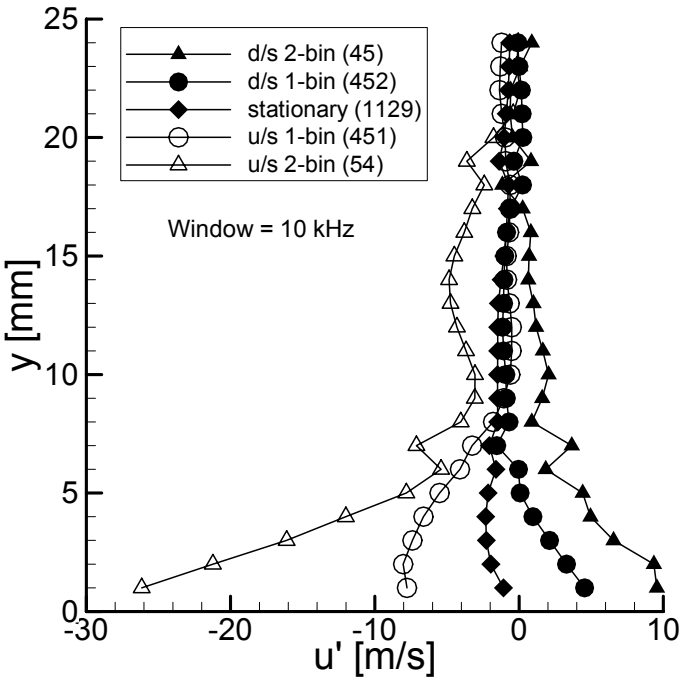

Figure 7. Conditional ensemble average profiles of the streamwise velocity fluctuations in the incoming boundary layer conditioned upon the separation shock foot motion within a time period corresponding to 4 kHz in a compression ramp-induced separated flow (Ref. 18).

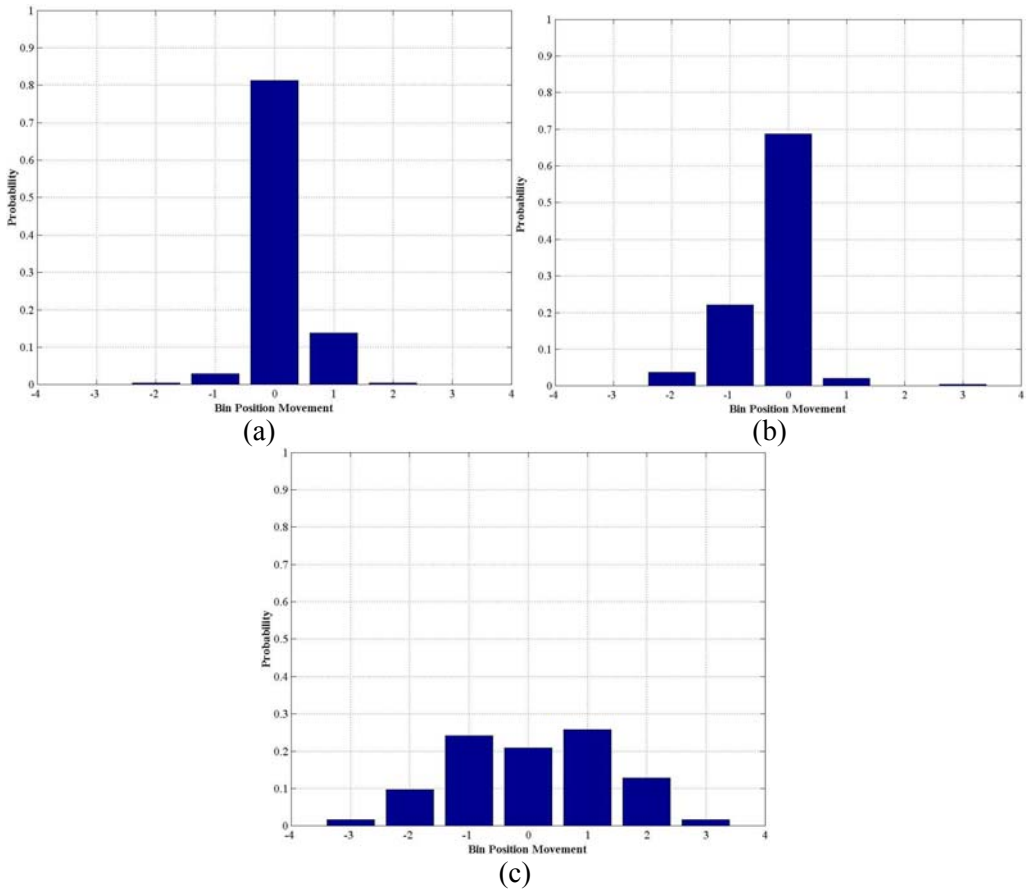

Figure 8. Conditional ensemble average histograms showing the probability of the shock foot movement during pulsed injection events. (a) shock movement resulting from turning injectors on, (b) movement resulting from turning injectors off, (c) movement without injection.

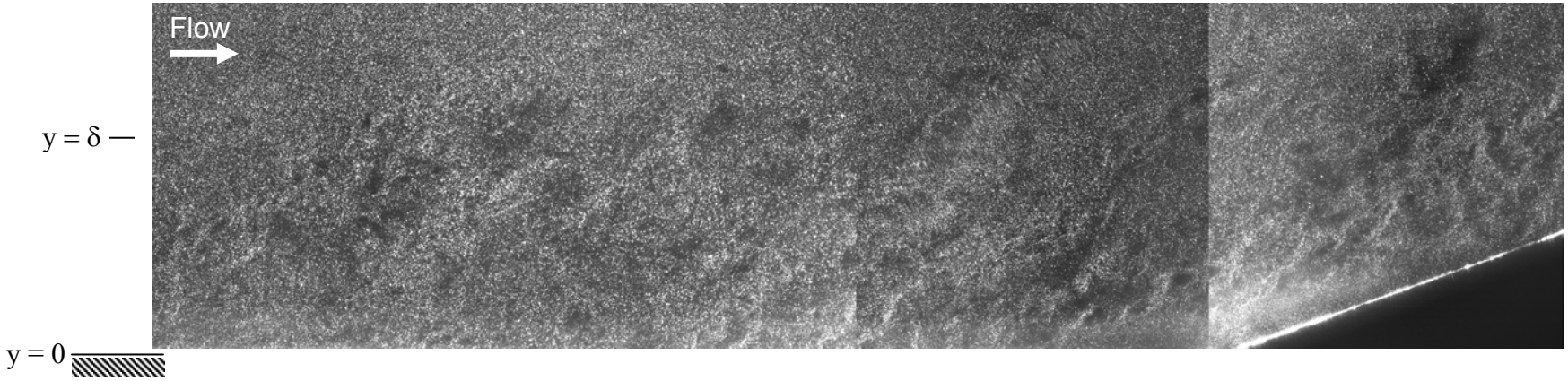

Figure 9. Sample single-pulse particle image for the 20 degree ramp and large field-of-view imaging.

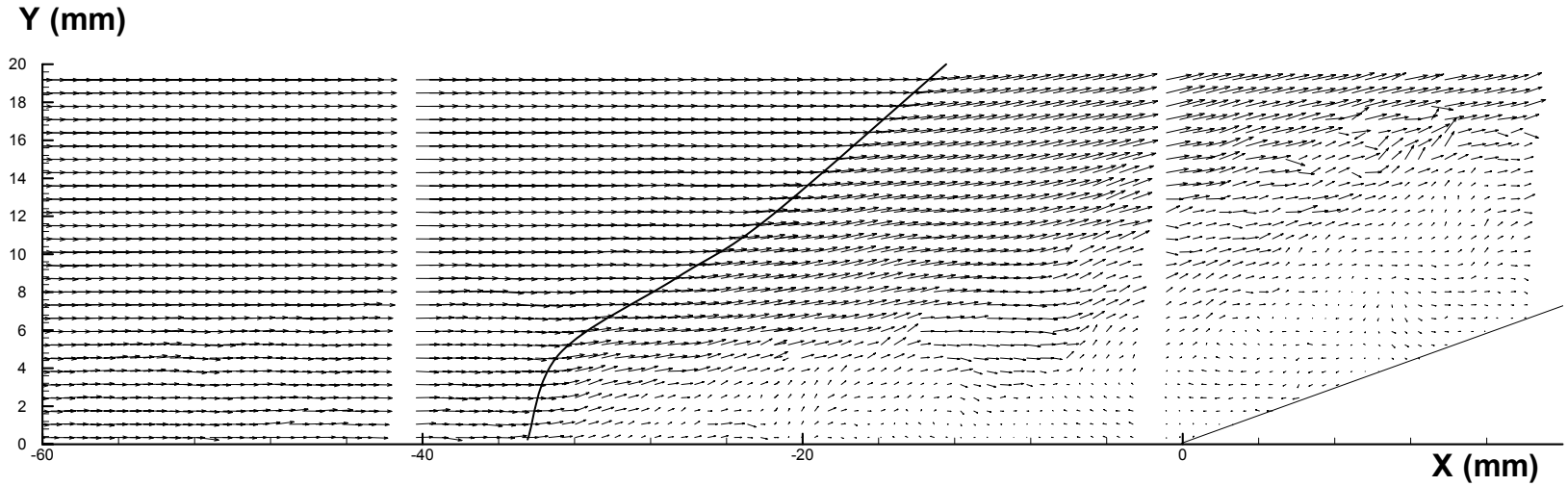

Figure 10. Instantaneous velocity vector field for the 20 degree ramp and large field-of-view imaging.

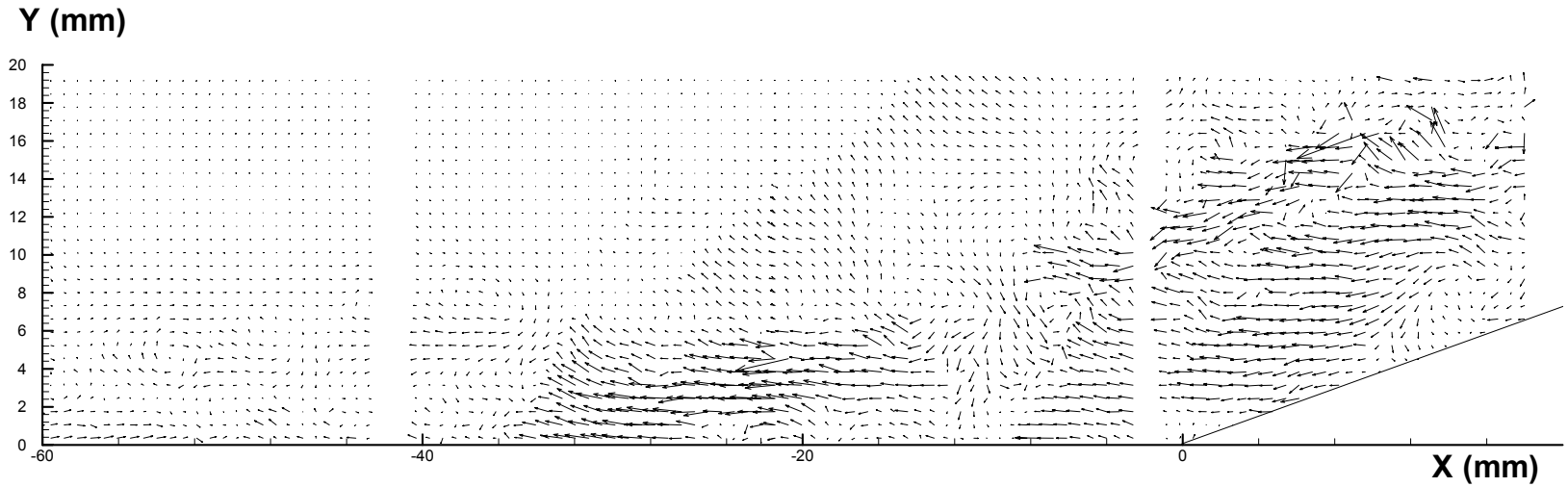

Figure 11. Velocity fluctuation vector field for the 20 degree ramp and large field-of-view imaging.

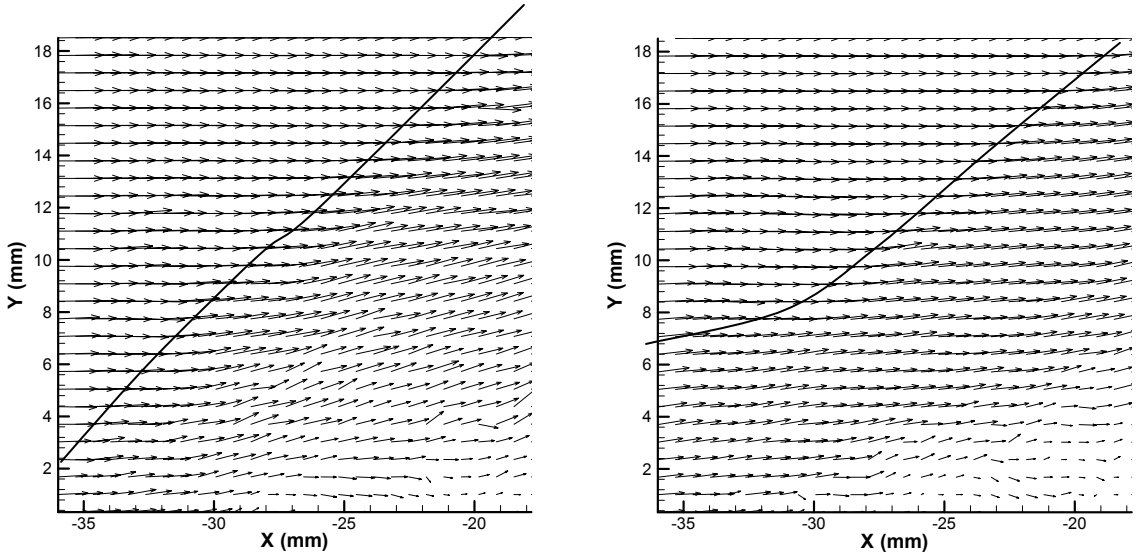

(a) (b)

Figure 12. Velocity vectors for time-sequenced PIV pairs separated in time by 40 μs. The image at right was taken 40 μs after the image at left.